NASA TECHNICAL NOTE

NASA TN D-2295

OTS: $0.75

NASA TN D-2295

30p.

N64-19726 * 1.B

CODE-1

Title

# DESIGN AND OVERALL PERFORMANCE OF AN AXIAL-FLOW-PUMP ROTOR WITH A BLADE TIP DIFFUSION FACTOR OF 0.43


*by James E. Crouse and Donald M. Sandercock*

*Lewis Research Center*

*Cleveland, Ohio*


Washington, NASA, May 1964
30p refs

1705771


NATIONAL AERONAUTICS AND SPACE ADMINISTRATION, • WASHINGTON, D. C. • MAY 1964

Lewis Research Center, Cleveland, Ohio

# DESIGN AND OVERALL PERFORMANCE OF AN AXIAL-FLOW-PUMP ROTOR WITH A BLADE TIP DIFFUSION FACTOR OF 0.43

By James E. Crouse and Donald M. Sandercock

Lewis Research Center
Cleveland, Ohio

NATIONAL AERONAUTICS AND SPACE ADMINISTRATION

For sale by the Office of Technical Services, Department of Commerce,
Washington, D.C. 20230 -- Price $0.75

# DESIGN AND OVERALL PERFORMANCE OF AN AXIAL-FLOW-PUMP ROTOR WITH A BLADE TIP DIFFUSION FACTOR OF 0.43

by James E. Crouse and Donald M. Sandercock

Lewis Research Center

A a C

## SUMMARY

An axial-flow-pump rotor was designed by a blade-element technique and tested in the Lewis Research Center water tunnel. The rotor design incorporated a hub-tip radius ratio of 0.7, diffusion factors of 0.43 at the tip and 0.69 at the hub, and radially constant energy addition. Blades of the circular-arc type with 1.5-inch chord length and with a tip solidity of 1.01 were used.

At the design flow coefficient (0.284) a measured overall head-rise coefficient of 0.282 and an overall efficiency of 0.937 were obtained. Both values were slightly higher than the design values. The curve for head rise as a function of flow coefficient shows that the design flow occurred very close to a limiting operating condition, as evidenced by excessive rig vibrations in the low-flow regime.

Operation at a constant tip speed of 142 feet per second and various inlet pressures indicated that cavitation begins to affect rotor performance when the net positive suction head is lowered to about 116 feet. At a flow coefficient of 0.390, this corresponds to a suction specific speed of approximately 7600 (blade cavitation number, approx. 0.191).

At all modes of operation (both cavitating and noncavitating), the close agreement between the radial distribution of measured axial velocity and that computed by simple radial equilibrium relations indicates the adequacy of the simple radial equilibrium expression to describe the radial distributions of flow.

## INTRODUCTION

For certain applications the axial-flow pump shows much promise; however, the background information from high-specific-speed pumps necessary to support a design system is meager. One source of this type of information is the low-speed-air cascade data that was incorporated into a design system for axial-

flow compressors (see ref. 1). A step toward determining the usefulness of the correlations of cascade and axial-flow-compressor data in a pump design system was taken by testing a pump whose design was based on the method advanced in reference 1. This axial-flow-pump rotor that utilized a hub-tip ratio of 0.4 was rather lightly loaded in the blade tip regions. Such a rotor would be similar to the type of stage located in the inlet portion of a multistage pump immediately downstream of an inducer. The results of the investigation presented in references 2 and 3 indicated a potential efficiency greater than 0.90, but that modification to the compressor design procedure may be necessary to achieve optimum performance.

In order to evaluate further blade loading limits (as applied to axial-flow pumps) as well as the utility of the information of reference 1, a second axial-flow rotor was designed in accordance with the method presented in reference 1. This second design incorporated higher blade loadings and a hub-tip ratio of 0.7. Both of these design conditions make the rotor typical of a stage located far enough downstream of the multistage pump inlet that loading limits rather than cavitation limits are of primary concern. This report presents the design, overall performance, and radial distributions of flow measurements at selected operating conditions of this 0.7-hub-tip-ratio rotor. Comparisons with design values, as well as with similar performance results observed in the investigation of the 0.4-hub-tip-ratio rotor, are made. Quantitative effects of neglecting radial flows in radial equilibrium calculations are investigated by applying the simple radial equilibrium expression

$$\frac{\partial h}{\partial r} = \frac{V_\theta^2}{gr} \tag{1}$$

to flow conditions at the rotor exit and by comparing the values obtained with measured values. (All symbols are defined in appendix A.)

## PUMP DESIGN

### General Design Philosophy

The general design procedure and philosophy follow those presented in reference 2 with only minor exceptions, which will be noted. In brief, the design utilized a blade-element concept whereby design conditions are computed across a number of individual blade elements at selected radial locations. Each element design is achieved by computing velocity diagrams at the blade inlet and outlet and then specifying a blade shape to establish the desired velocity diagrams. Finally, the complete blade is obtained by stacking the individual blade elements in some suitable fashion.

Ideally, a blade element would lie on a surface generated by rotating a streamline about the axis of rotation; however, since flow conditions (velocity diagrams) are computed only at blade inlet and outlet stations, the blade element is assumed to lay on a conical surface between the radial locations at which the streamline intersects the computational stations at the blade inlet and outlet. Because this design utilized constant hub and tip diameters

across the rotor, assumed the inlet axial velocity constant across the passage, and calculated very small radial shifts of streamlines across the blade (see design distribution of outlet flow coefficient in fig. 7, p. 10), the blade elements were further simplified by the assumption that they lay on cylindrical surfaces.

## Selection of Velocity Diagrams

The inlet conditions were chosen to be the same as those for the 0.4-hub-tip-ratio rotor, whose performance is reported in references 2 and 3, in order to reduce the variables affecting comparisons of performances. The ideal inlet flow coefficient is considered to be constant in magnitude ($\varphi_i = 0.294$) and axial in direction at all radii. These combine to give a design inlet relative flow angle at the blade tip of $73.6^{\circ}$ and permit calculation of inlet velocity diagrams at all radii.

Under real flow conditions a certain amount of flow blockage will be realized from the hub and tip casing boundary layers. In this design the blockage was assumed to be 3 percent; that is, the inlet velocity diagrams will be achieved in the free-stream flow area when the measured flow coefficient $\varphi$ is

$$\varphi = 0.97 \times \varphi_i = 0.284$$

The computation of the outlet velocity diagrams follows the procedure of reference 2 and is not repeated in detail herein. The calculated head rise results from the selected values of blade loading and loss. In addition, from considerations of mixing losses, it is desired that the head rise should not vary markedly with radius. A measure of the blade loading is obtained from the blade diffusion factor D, defined and developed in reference 4 as

$$D = 1 - \frac{V_2'}{V_1'} + \frac{\Delta V_\theta'}{2\sigma V_1'} \tag{2}$$

In preliminary design calculations a blade diffusion factor of 0.70 at the blade hub was selected. If it is assumed that there were no changes in axial velocity across the blade row, an ideal head-rise coefficient (energy addition) at the hub section may be computed. Maintaining a constant ideal head-rise coefficient at all radii allows preliminary values of the blade diffusion factor and velocity diagrams at each blade element to be computed. The values of blade diffusion factor are used to aid in establishing a radial variation of loss coefficient from the results of reference 1 (curve of blade diffusion factor against loss coefficient) and are tempered by the comparative results shown in reference 3. Using this radial distribution of loss coefficient, a constant ideal head-rise coefficient, and assuming that radial equilibrium may be expressed by

$$\frac{\partial h}{\partial r} = \frac{V_\theta^2}{gr} \tag{3}$$

yields the outlet axial velocity at all radii computed from equation (B4b) of appendix B. With this new distribution of axial velocity, the calculation pro-

cedure is repeated until a satisfactory radial distribution of velocity diagrams is obtained.

In the final design, the blade diffusion factor varied from 0.69 at the hub to 0.43 at the blade tip. An ideal head-rise coefficient of 0.294 was maintained across the passage with radially varying values of outlet flow coefficient, loss coefficient, and head-rise coefficient. Radial distributions of design velocity diagram parameters are shown in the following table for an ideal inlet flow coefficient of 0.293, an inlet flow angle of 0, and an ideal rotor head-rise coefficient of 0.294:

| Rotor hub-tip radius ratio, $r/r_t$ | Outlet flow coefficient, $\varphi_2$ | Relative inlet flow angle, $\beta_1'$, deg | Change in relative flow angle, $\Delta\beta'$, deg | Rotor head-rise coefficient, $\psi$ | Loss coefficient, $\bar{\omega}$ | Blade diffusion factor, D |
|---|---|---|---|---|---|---|
| [a]1.00 | 0.233 | 73.6 | 1.8 | 0.238 | 0.0750 | 0.426 |
| .95 | .305 | 72.8 | 8.4 | .279 | .0425 | .433 |
| .90 | .312 | 71.9 | 10.4 | .281 | .0428 | .464 |
| .85 | .308 | 70.9 | 12.5 | .280 | .0496 | .505 |
| .80 | .297 | 69.8 | 14.4 | .273 | .0649 | .555 |
| .75 | .281 | 68.6 | 16.8 | .263 | .0869 | .615 |
| [b].70 | .254 | 67.2 | 19.5 | .249 | .1221 | .693 |

[a]Tip.
[b]Hub.

Overall mass-averaged values of head-rise coefficient $\bar{\psi}$ and efficiency $\bar{\eta}$ are 0.269 and 0.917, respectively. Both of these values are based on blade-element design values and do not contain any boundary-layer correction (see ref. 1, ch. VIII).

If it were desired to repeat this type of stage in a multistage application, a set of stator blades to set up necessary inlet flow conditions to the succeeding rotor would be required. In order to determine the level of blade loading on such a stator row, a simple calculation of stator diffusion factors was made. Stator diffusion factors of approximately 0.59 and 0.69 at the blade tip and hub, respectively, were calculated with the assumptions that

(1) Stators return fluid to the axial direction

(2) Stator blade solidity at the tip is 1.0 and the chord is constant

(3) A radially constant outlet velocity equal to the rotor inlet velocity is attained

At present, stator performance data are too meager to determine whether such blade diffusion factors are attainable without excessive losses.

## Selection of Blading

Once the velocity diagrams have been established, the next step is the selection of a blade shape to achieve the desired flow conditions. For this design, the double-circular-arc blade was utilized (the blade shape selected for the 0.4-hub-tip-ratio rotor reported in ref. 2).

Blade incidence and deviation angles were computed from the equations of reference 1 (ch. VII) with the following modifications:

(1) The value of the correction term $i_c - i_{2-D}$ was based on the pump performance data reported in reference 2. From the results of this investigation a $3^{\circ}$ correction was applied at all radii.

(2) In the tip region calculations from the design equations indicated a very high incidence angle and negative camber and deviation angles. Because these values are unrealistic, the tip element design was modified to give a blade with zero camber, and the same deviation angle was assumed as was computed for the element 10 percent of the passage height from the tip.

A blade chord of 1.5 inches was selected based on considerations of the number of blades and the desired solidity. Blade mean-line camber angles were computed from the standard formula

$$\Phi = \Delta\beta' - i + \delta \tag{4}$$

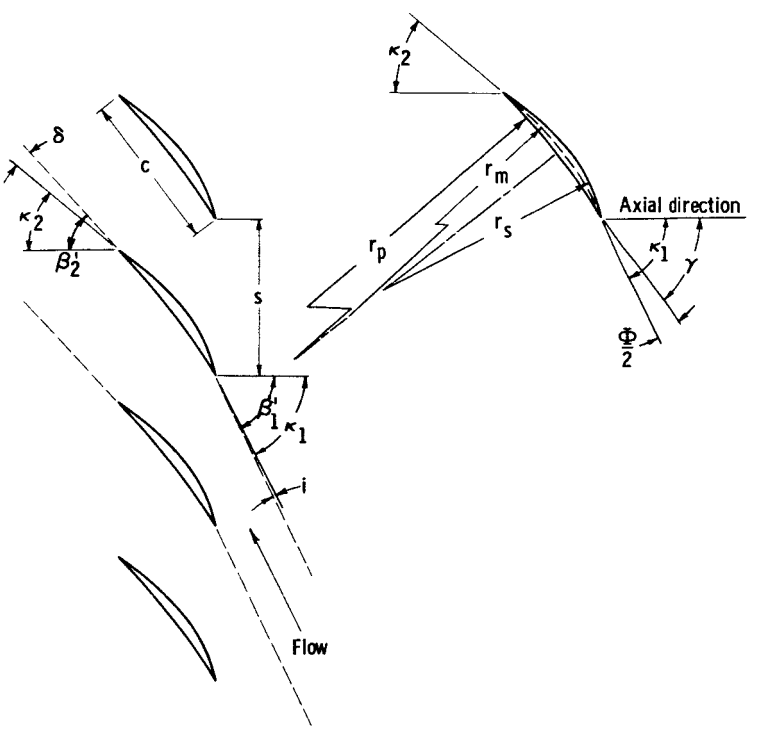


Figure I. - Blade nomenclature.

The suction and pressure surfaces were established by the circular arcs passing through the point of maximum-thickness and tangent to 0.010-inch-radius circles forming the leading and trailing edges. The chosen blade maximum thickness (percent of chord) varied linearly from 7 percent at the tip to 8.5 percent at the hub. These blade sections were then stacked so that the centers of gravity of the individual blade sections formed a radial line from the axis of the rotor. The blade nomenclature is shown in figure 1, and pertinent design values are listed in the following table for a rotor tip diameter of 9.00 inches, 19 blades, and a blade

chord of 1.52 inches:

| Rotor hub-tip radius ratio, $r/r_t$ | Incidence angle, i, deg | Deviation angle, $\delta$, deg | Camber angle, $\Phi$, deg | Solidity, $\sigma$ | Setting angle, $\gamma$, deg | Ratio of maximum thickness to chord, $t_{max}/c$ |
|---|---|---|---|---|---|---|
| [a]1.00 | 6.4 | 4.6 | 0 | 1.01 | 67.1 | 0.0700 |
| .95 | 2.0 | 5.4 | 11.8 | 1.06 | 64.9 | .0725 |
| .90 | .9 | 6.9 | 16.4 | 1.12 | 62.8 | .0750 |
| .85 | .5 | 7.8 | 19.8 | 1.19 | 60.5 | .0775 |
| .80 | .6 | 8.3 | 22.1 | 1.26 | 58.2 | .0800 |
| .75 | 1.0 | 8.8 | 24.6 | 1.35 | 55.3 | .0825 |
| [b].70 | 1.2 | 9.3 | 27.6 | 1.44 | 52.2 | .0850 |

[a]Tip.

[b]Hub.

The blades were manufactured individually and inserted in the rotor (fig. 2).

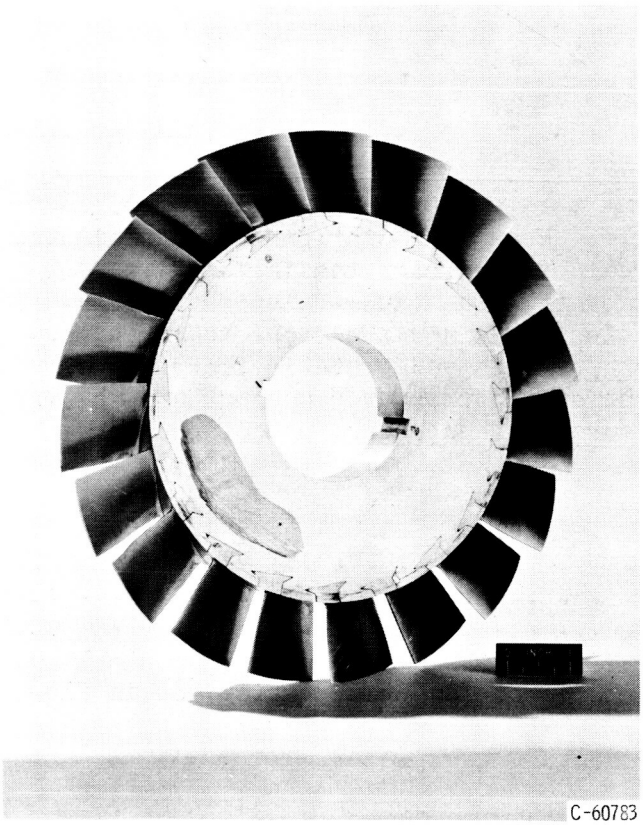


Figure 2. - Rotor.

## APPARATUS AND PROCEDURE

### Test Facility

The pump was tested in the Lewis water tunnel, which is shown schematically in figure 3. Since the pump installation is described in detail in reference 2, it will not be discussed herein. During the tests, the gas content of the water was maintained below 3 parts per million by weight. The filtering system was capable of removing solid matter larger than 5 microns.

### Instrumentation

The instrumentation can be divided into two groups: (1) instruments used to obtain overall test loop or general conditions and (2) survey instruments used to obtain detailed blade-element data. The test loop instrumentation consisted of a venturi flowmeter, an electronic speed counter used in conjunc-

tion with a magnetic pickup, an automatic water temperature control and recorder, and a pressure transducer with the associated power and recording equipment to measure the loop pressure. The survey instruments (fig. 4) con-

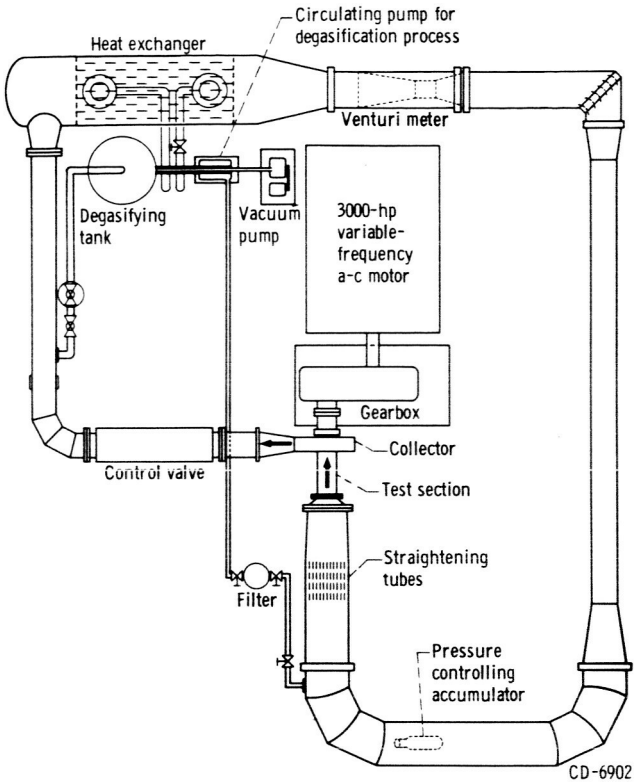


Figure 3. - Lewis water tunnel.

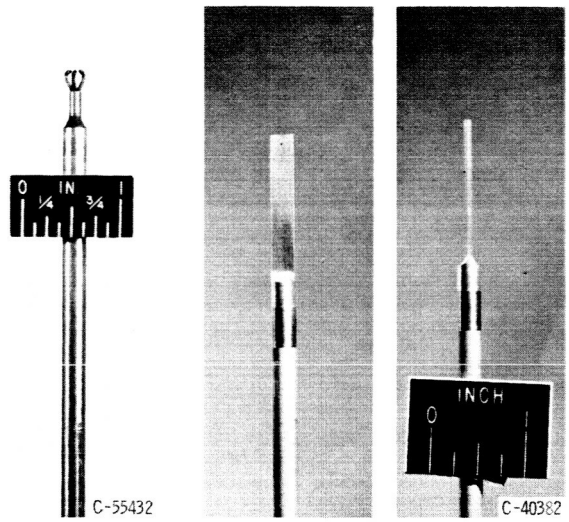


(a) Total-pressure claw.

(b) Static-pressure wedge.

Figure 4. - Probes.

sisted of a claw-type probe for measuring total head and angle and a wedge-type probe for measuring static head and angle. Measuring stations were located approximately 1 inch upstream and downstream of the rotor leading and trailing edges, respectively. Each claw and wedge utilized a null-balancing stream-direction-sensitive element that automatically alined the probe to the direction of flow. A head calibration factor for each wedge static probe was determined in an air tunnel and applied to the static pressures measured in the water tunnel. The inherent accuracies of measurement and recording devices were the following:

| | |
|---|---|
| Flow rate, Q, percent . . . . . | < ±1.0 |
| Rotative speed, N, percent . . . . . | ±0.5 |
| Differential heads, $\Delta H$, ft . . . . . | ±1.0 |
| Flow angle, $\beta$, deg . . . . . | ±0.5 |

No evaluation of measurement errors due to circumferential variations in flow, unsteady flows, etc. was attempted.

## Procedure

Characteristic performance curves were obtained by operating the rotor at constant rotative speed and net positive suction head over a range of flow control valve settings. The data were taken by surveying total and static heads, and flow angles across the annulus at preprogramed radial positions located at approximately 10, 30, 50, 70, and 90 percent of passage height from the tip. The data presented were taken along characteristic curves for the following conditions:

| Rotor tip speed, $U_t$, ft/sec | Net positive suction head, $H_{s,v}$, ft |
|---|---|
| 113 | 132 |
| 142 | >160 |
| 142 | 116 |
| 142 | 89 |
| 142 | 72 |

The equations used to calculate the selected performance parameters are presented in appendix B.

Some check on the reliability of the data may be obtained from figure 5,

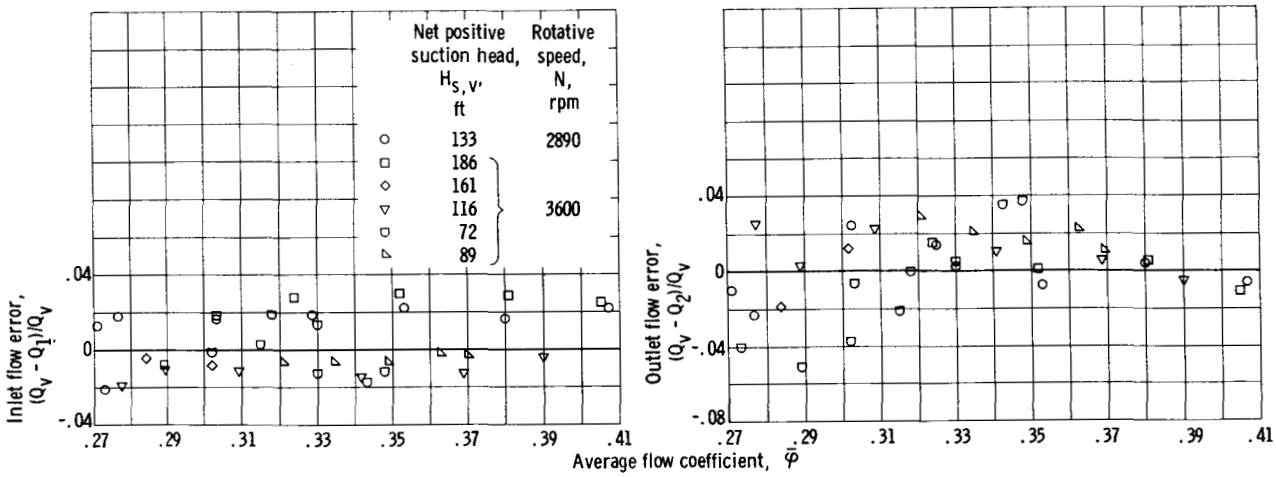


(a) Inlet measuring station.

(b) Outlet measuring station.

Figure 5. - Comparison of integrated weight flows at blade inlet and outlet with those measured by venturi meter.

where the integrated weight flows at the blade inlet and outlet are compared with those measured by the venturi flowmeter. The data are presented in the form of a difference of the two flows (as a fractional portion of the venturi flow) as a function of inlet flow coefficient. Good comparisons were obtained at the inlet and the outlet measuring stations.

## RESULTS AND DISCUSSION

In the presentation of the results, data for noncavitating and cavitating conditions are discussed in separate sections. In this investigation, cavitaing and noncavitating flow regimes were determined in the following manner with the pump operating at design speed (blade tip speed of 142 ft/sec):

(1) The pressure level in the tunnel was raised to the highest value considered safe with the Lucite casing. At this operating condition, some cavitation remained in the vortex caused by the blade-tip clearance flow (see ref. 5) but no blade surface cavitation could be observed.

(2) As the inlet pressure was reduced, the cavitation in the tip vortex increased slightly, and blade surface cavitation at the blade leading edge could be observed; however, no reduction in the head rise measured across the blade tip region could be observed until the inlet pressures were reduced to a value of approximately 120 feet. To obtain noncavitating performance, the pump was operated at an inlet pressure greater than 160 feet. Although some tip vortex cavitation existed at this inlet pressure, it appears reasonably certain that the performance levels achieved would not measurably change with increased inlet pressures. Cavitation performance was measured over a range of net positive suction head down to 72 feet.

### Noncavitating Performance

Overall performance. - Head-rise coefficient and efficiency are plotted in figure 6 as functions of inlet flow coefficient to show overall noncavitating

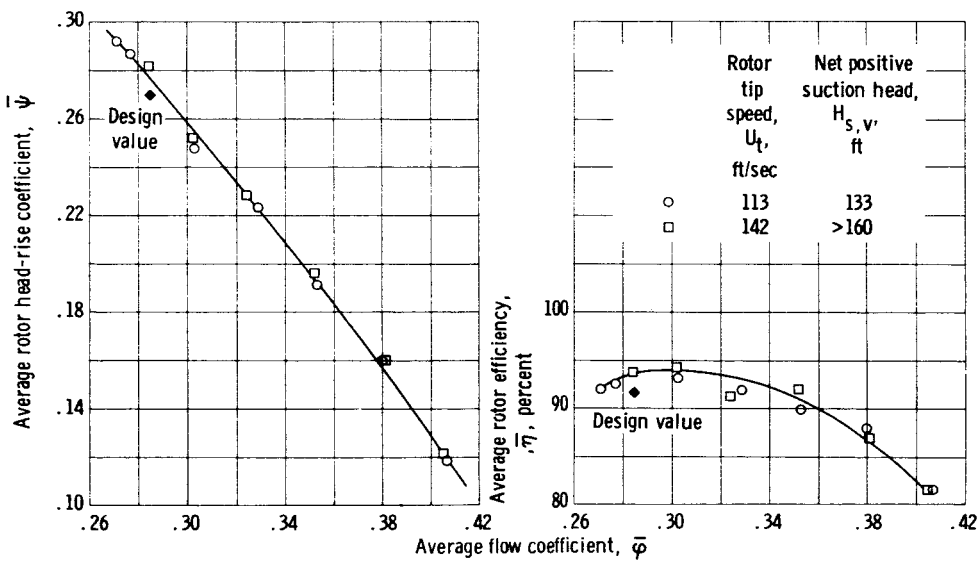


Figure 6. - Overall performance of axial-flow-pump rotor for noncavitating conditions.

performance. The head-rise coefficient and efficiency represent mass-averaged values, while the flow coefficient is an average value based on venturi measured flows and inlet geometric area. For comparative purposes, design values are included. Flow range was limited at the high flows by system flow losses

and at the low flows by rig vibrations deemed by the operator to be excessive for any extended operation. Over the range of flows tested, the characteristic head-rise-flow curve shows the inverse and nearly linear relation typical of the axial-flow stage reaching a maximum averaged head-rise coefficient of 0.292 at a flow coefficient of 0.271.

The rotor attained a maximum efficiency of approximately 0.94 at a flow coefficient of 0.302 (slightly higher than design) and showed an efficiency of 0.90 or greater over approximately 60 percent of the flow range covered. Even at the low flow cutoff, where blade stall is probably occurring, an efficiency greater than 0.90 was measured. Reduced efficiencies (<0.90) occurred in the high-flow range of operation.

The data presented in figure 6 were obtained at two different speeds. Reynolds numbers based on blade chord and blade-tip speed varied from $1.61\times10^6$ to $2.10\times10^6$. Over this range of Reynolds number, the data taken in this investigation show no measurable differences in either head-rise coefficient or efficiency. In reference 2, results were noted for a Reynolds number range of $1.09\times10^6$ to $2.18\times10^6$. In contrast, the performance results of reference 6 for a flat-plate helical inducer, although showing no observable differences in head-rise coefficient, did exhibit variations in the measured efficiencies for

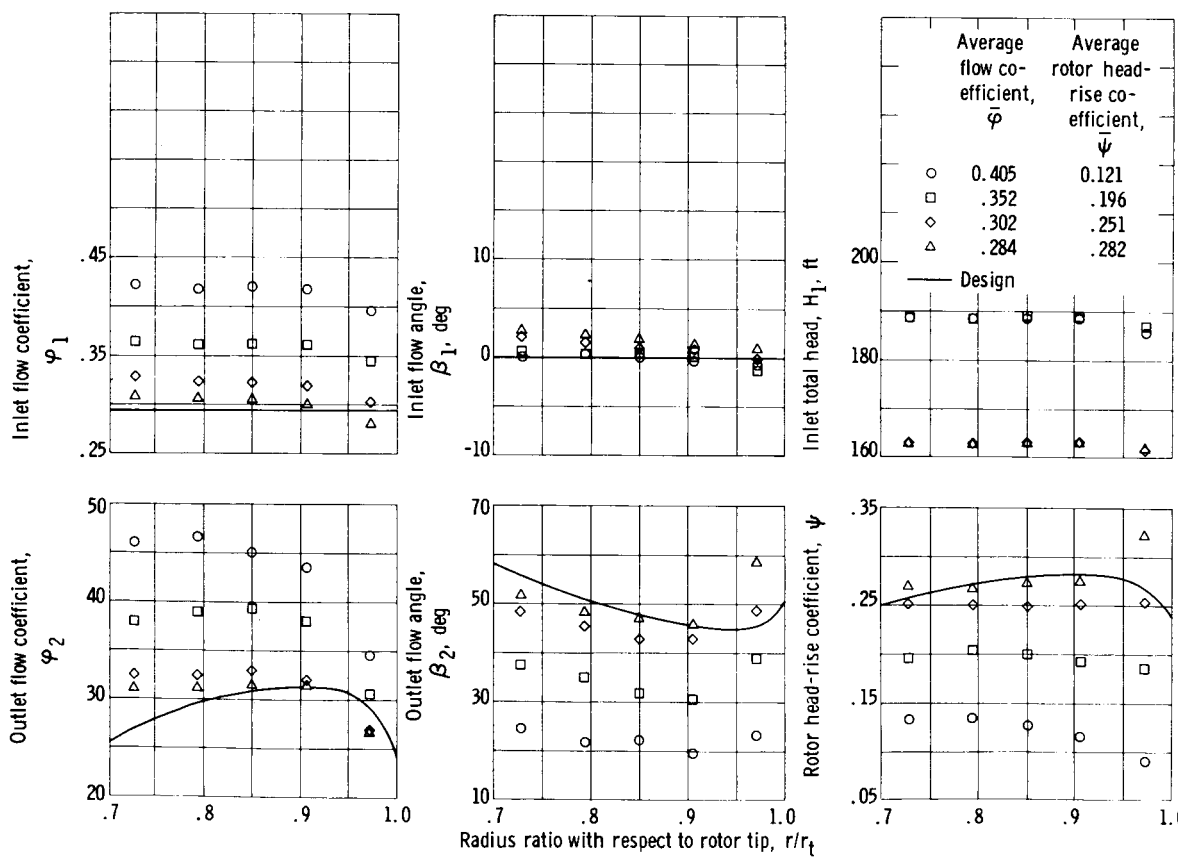


Figure 7. - Radial distributions of flow and performance parameters for noncavitating conditions. Blade tip speed, 142 feet per second.

the Reynolds number range from $1.85 \times 10^7$ to $3.7 \times 10^7$.

At the design flow point (which includes an assumption of a 3-percent boundary layer blockage) a mass-averaged head-rise coefficient of 0.282 was measured compared with the design value of 0.269. At this operating condition the rotor efficiency was 0.937, which is slightly higher than the 0.917 value anticipated in the design. It is also notable that the design point occurred very close to the lower limit of the flow range.

Radial distributions. - Shown in figure 7 are typical radial distributions of the measurements obtained from the passage surveys for various modes of operation with parameters that directly reflect the value of the measurements. These include radial distributions of flow angles and flow coefficients at inlet and outlet measuring stations, inlet total head, and head-rise coefficient. The data were obtained at a rotor tip speed of 142 feet per second.

At all operating conditions, the radial distributions of inlet parameters were similar. Inlet flow angles indicated that the inlet flow was within $\pm 3^{\circ}$ of the axial direction (compared with the design assumption of inlet flow angle equal to zero) at all flow coefficients. Both the inlet total head and the flow coefficient showed slight reductions in the tip region, but were essentially constant over the remainder of the flow passage. Since the tip-element measuring station was within approximately 1/8 inch of the outer wall, the effects of the boundary layer at the outer casing were probably being felt at this radial location.

The radial distributions of parameters at the blade outlet reflect the variations that may be expected for a design of this type over a range of operating conditions. In this case most of the usable flow range fell on the high flow side of the design point. Just as observed in other investigations of axial-flow rotors with axial inlet flow, the greatest changes in head rise with flow coefficient occur in the tip regions, the differences decreasing with radius. This can be at least partly explained by a velocity diagram study which shows that, (with the assumption that deviation angle does not vary with flow) for a given change in inlet axial velocity (flow coefficient), the greatest variation in outlet tangential velocity (hence energy input) will occur for the diagram with the highest inlet relative flow angle. Of course, the measured head rise depends on both the energy addition and loss. The axial velocity, or flow coefficient, distributions are those necessary to satisfy continuity and radial equilibrium requirements.

A salient feature of the performance map of any rotor is the flow margin between design point operation and the point where blade stall occurs. It was noted in the section Overall Performance that the design point lay close to the inlet flow coefficient at which operation had to be terminated because of excessive rig vibrations (fig. 6, p. 9). The design blade loading is considered relatively high, and the radial distribution of inlet flow coefficient (incidence angle) and the head-rise coefficient indicate that, at design flow, the blade tip region is operating at a blade loading higher than the design values. Thus, at least in the tip region, the flow range between design and blade stall could be small. Reference 7 shows that for the 65 series airfoil in cascade the stall angle of attack moves progressively closer to the design value with

increasing section camber (blade loading). It shows further, that for a given blade camber, the operating angle-of-attack range decreases as inlet angle increases. Whether the excessive rig vibrations could have been caused by blade stall in the tip region alone or by complete blade stall, which, once initiated in the tip region, would quickly spread across the complete blade height in this high-hub-tip-ratio blade row, could not be determined. An additional unknown is the effect of higher blade loading on the vortex arising from tip-clearance flows. One specific conclusion from the data shown is the need for accurately defining inlet flow conditions and for closely predicting minimum-loss incidence angles when utilizing highly loaded, high-inlet-angle rotor rows.

For comparison with design, the results obtained at a flow coefficient of 0.284 are used (see fig. 7, p. 10). As the inlet-flow-coefficient distribution indicates, the rotor was operating at a slightly higher than design flow coefficient (lower than design incidence angle) at all radial locations except the tip, where a flow coefficient lower than the design value (incidence angle higher than design) was indicated. The rotor produced a head-rise coefficient close to the design value at all radii except in the tip region, where a value of head rise significantly higher than the design head rise was observed. In this region, the outlet flow coefficient and the outlet flow angle suggest that the energy addition (see eq. (B1)) was also significantly larger than the design value. The value of the mass-averaged head-rise coefficient higher than the design value noted in figure 6 is evidently a result of this tip operating condition.

## Cavitating Performance

As mentioned earlier, the primary purpose of a stage like that tested is to produce a maximum head rise. Although the rotor is generally located in a multistage pump where it is free of cavitating conditions, there are problems of design and operation that may require some knowledge of the cavitation performance of the rotor. These problems include

(1) The value of net positive suction head or, more fundamentally, the blade cavitation number at the inlet of a rotor with this blade geometry and level of loading at which cavitation initially affects rotor performance.

(2) The degree to which performance and/or flow range of such a stage would be adversely affected if, for some short period of time during startup, acceleration, loss of tank pressure, etc., the inlet pressure to the stage were seriously reduced. To aid in solving this type of problem, some cavitation performance data for the test rotor are presented in the following sections.

Overall performance. - Plots of head-rise coefficient and efficiency against flow coefficient at several values of net positive suction head are shown in figure 8. The plots present the overall cavitating performance of the rotor and, for comparison, the noncavitating performance. Data were obtained at a blade tip speed of 142 feet per second. All parameters represent averaged values defined by the appropriate equations of appendix B.

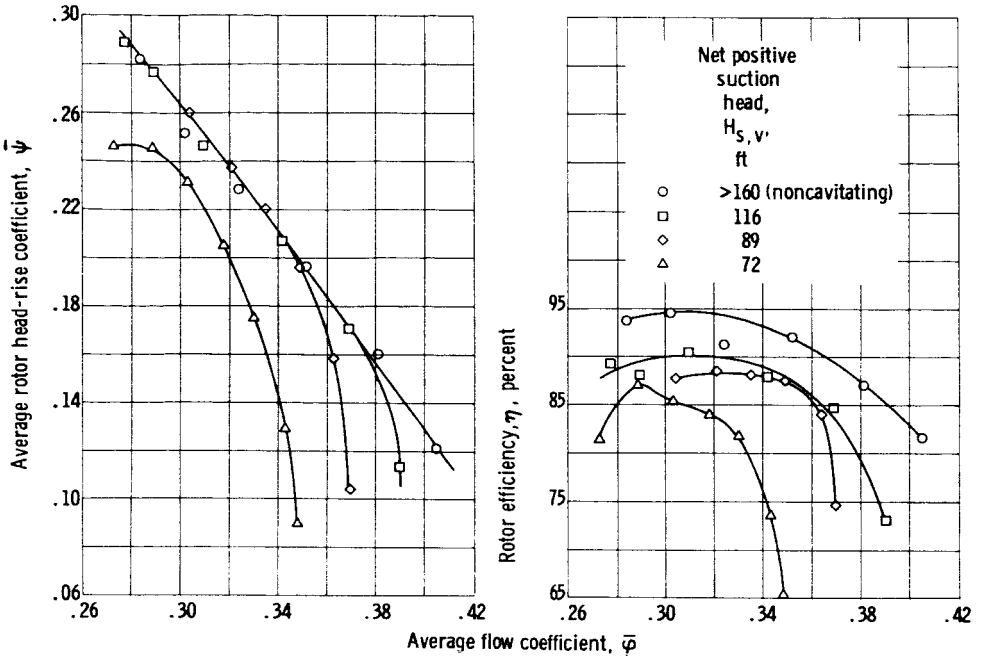


Figure 8. - Overall performance of axial-flow-pump rotor for cavitating conditions.

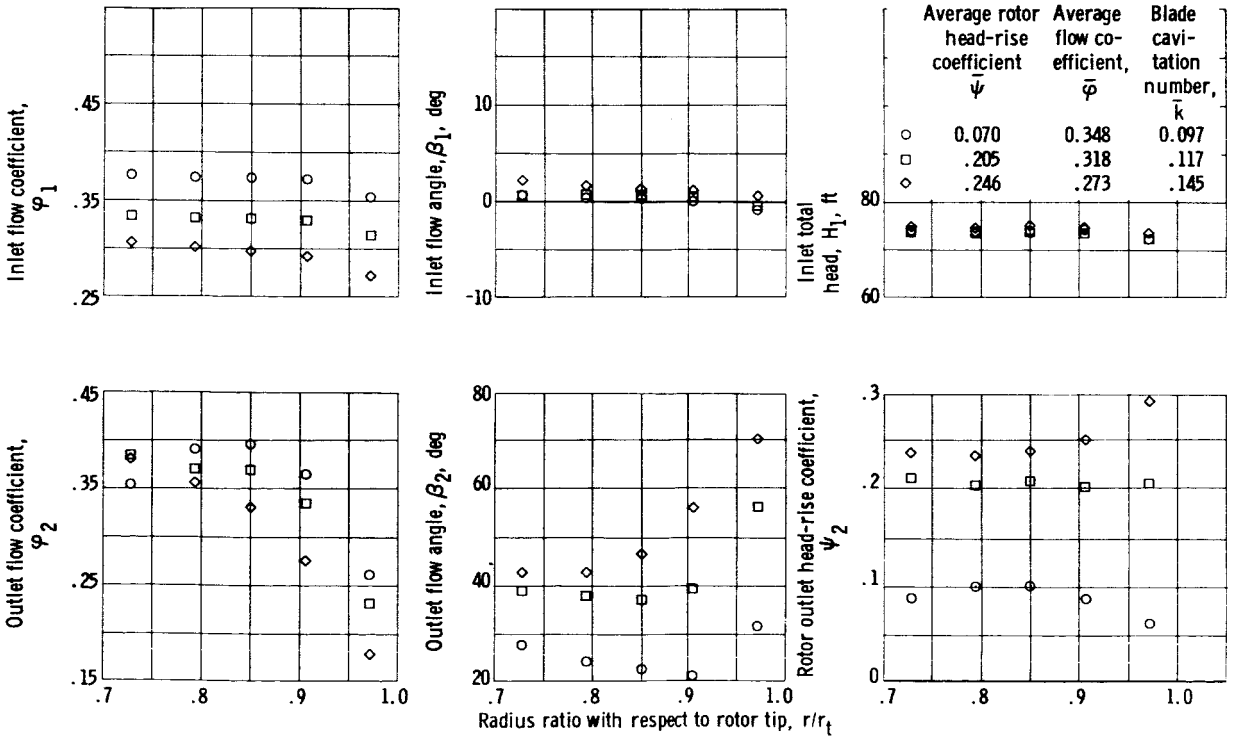


Figure 9. - Radial distributions of flow and performance parameters for cavitating conditions. Blade tip speed, 142 feet per second; net positive suction head, 72 feet.

For the range of operating conditions considered, the overall head-rise coefficient was initially affected at a net positive suction head of 116 feet. For this value and a blade tip speed of 142 feet per second, the maximum suction specific speed and the minimum cavitation number (both of which occur at the maximum flow coefficient of 0.390) would be approximately 7600 and 0.191, respectively. As the net positive suction head was decreased further, reductions in the head-rise coefficient from the noncavitating values were increased and extended over larger portions of the flow range. The overall flow range was also reduced. At design point (average inlet flow coefficient of 0.284), no loss of rotor head rise was encountered until a net positive suction head less than 89 feet was reached. In general, the efficiency decreases with net positive suction head at all flow conditions.

Radial distributions. - In figure 9, the radial distributions of selected parameters at the rotor inlet and outlet are presented for three modes of operation under cavitating conditions (net positive suction head of 72 ft). Blade cavitation numbers ranged from 0.097 (suction specific speed of 10,220) to 0.145 (suction specific speed of 9009). Evaluation of the effects of this degree of cavitation on these parameters can be made by comparing these results with the noncavitating data of figure 7 (p. 10).

The radial distributions of parameters at the rotor inlet are similar to those noted in figure 7 for noncavitating operation. This indicates that the inlet flow geometry need not be affected appreciably by rotor cavitation.

The radial distributions of head-rise coefficient are similar to the noncavitating variations for a given flow condition but are for a lower level of head rise. Decreases in head-rise coefficient due to cavitation occurred at all radii and approximately to the same degree or percentage.

The outlet flow coefficients show decreases in the tip region under cavitating conditions that were generally larger than those noted for similar noncavitating operation. At the low inlet pressure (net positive suction head of 72 ft) cavitation in the tip vortex was increased and presented increased blockage to flow in the tip regions. Also, radial equilibrium requirements changed from those observed at higher inlet pressures (net positive suction head greater than 160 ft), and flow shifts occurred to satisfy equilibrium conditions and continuity. Relative effects of these phenomena on the radial distribution of flow coefficient could not be evaluated.

At any exit radius the flow coefficient may be used in conjunction with the flow angle to give an indication of the work input by the rotor (see eq. (B1)). Comparison of the curves of figures 7 and 9 indicates that one of the effects of cavitation at all operating conditions is to decrease the energy input by the blade.

## Application of Simple Radial Equilibrium Equation

In the design of the test rotor, simple radial equilibrium (eq. (B4b)) was assumed to define the flow conditions. The validity of this assumption can be estimated by utilizing the measured flow angles and total head distribution in

the simple radial equilibrium equation (eq. (B5)) to calculate axial velocity distributions. The calculation procedure consisted in assuming tip axial velocities in an iterative process until flow continuity was achieved. A comparison of calculated axial velocity distributions by simple radial equilibrium (eq. (B5)) with the experimentally measured axial velocity distributions at a blade tip speed of 142 feet per second is presented for the following net positive suction heads and flow coefficient:

| Net positive suction head, $H_{s,v}$, ft | Flow coefficient, $\varphi$ |
|---|---|
| >160 | 0.405<br>.352<br>.302<br>.284 |
| 72 | 0.348<br>.318<br>.273 |

These comparisons (shown in fig. 10) indicate that the simple radial equilibrium expression adequately describes the axial velocity gradiant at all noncavitating and cavitating modes of operation tested.

## Rotor Performance Comparisons

In figures 11 to 13, the performance of the rotor reported herein is compared with that of the rotor used in the investigation reported in references 2 and 3. At equal radii, both rotors had the same design inlet flow coefficient, blade shape, solidity, chord length, and blade thickness (see the following table).

| Rotor | Hub-tip radius ratio, $r_h/r_t$ | Diffusion factor, D | | Radius ratio, $r/r_t$ | | |
|---|---|---|---|---|---|---|
| | | Hub | Tip | 1.0 | 0.7 | 0.4 |
| | | | | Ratio of maximum blade thickness to blade chord, $t_{max}/c$ | | |
| Present investigation | 0.7 | 0.69 | 0.43 | 0.07 | 0.085 | ---- |
| Ref. 2 | .4 | .60 | .25 | .07 | .085 | 0.10 |

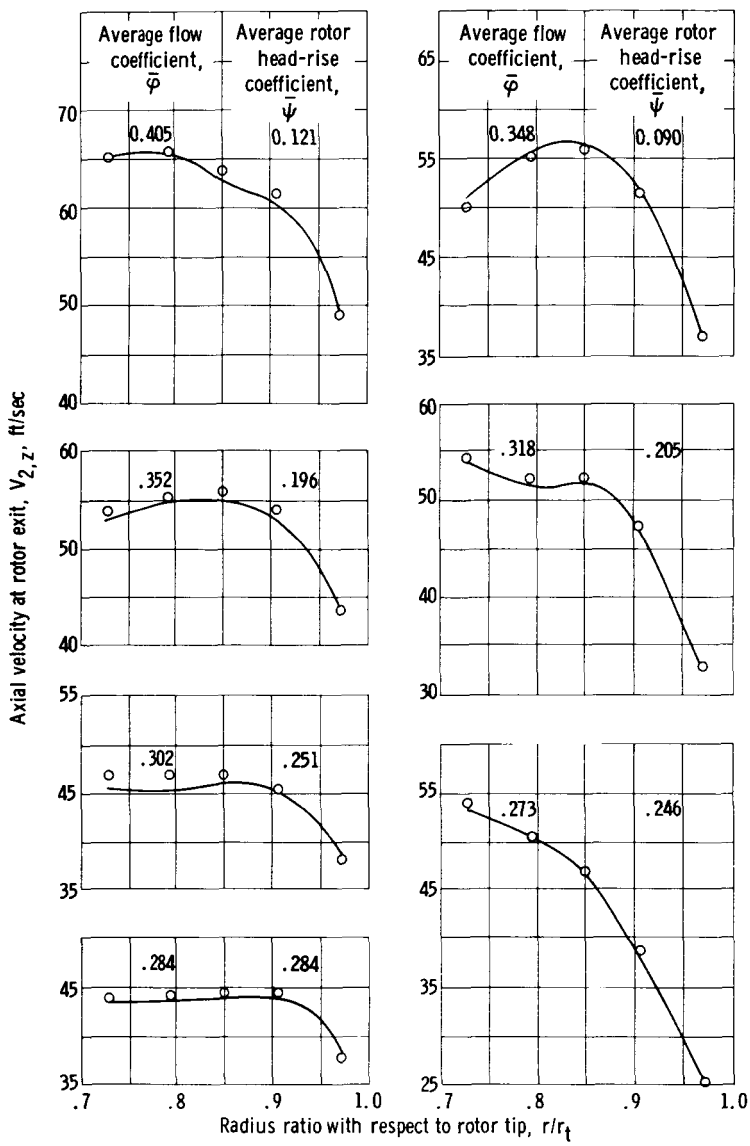


(a) Noncavitating condition.

(b) Cavitating condition; net positive suction head, 72 feet.

Figure 10. - Comparison of measured axial velocity distribution behind rotor with axial velocity distribution calculated by simple radial equilibrium.

Essentially the same design procedures were used for both rotors. Principal differences were in the hub-tip ratios and the design level of loading.

The overall performance of the two rotors is compared in figure 11, and the radial distributions of certain flow and performance parameters are compared in figures 12 and 13. The performance data for the 0.4-hub-tip-ratio rotor were taken from reference 3.

Both rotors exhibit characteristic curves typical for this type of pump rotor with the 0.7-hub-tip-radius-ratio rotor showing a steeper slope of the curve of average rotor head coefficient against average flow coefficient. The most encouraging comparison is the high level of efficiency and large flow range over which an efficiency of 0.90 or greater was obtained for the 0.7-hub-tip-ratio rotor which is highly loaded compared with the rotor of reference 3. It should be noted, however, that the blade elements of the 0.4-hub-tip-ratio rotor were not well matched and that a higher efficiency potential exists for this type of rotor than that shown by the measured data (see ref. 3).

A second significant comparison involves the proportion of flow range on either side of the design point. Generally, it would be desirable for the design point to fall close to the middle of the stable operating range and to occur close to maximum efficiency. Each of the rotors displays one of these two desirable operating conditions. Reference 3 shows that, at design flow coefficient, the design incidence angles (approx. $0.5^{\circ}$ to $3.0^{\circ}$) are lower than the observed minimum-loss incidence angles (approx. $3^{\circ}$ to $4^{\circ}$), which occur at a flow coefficient lower than the design values. Under these conditions, the flow range, or incidence angle, between design and blade stall would be increased, but the design point efficiency would be lower than maximum efficiency,

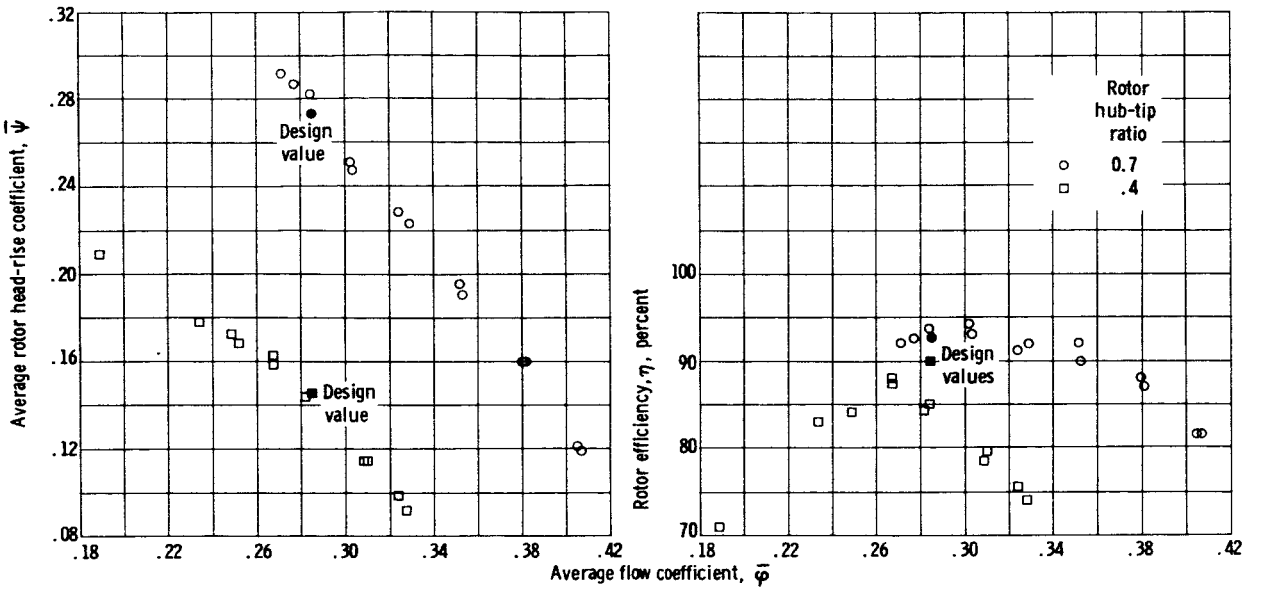


Figure 11. - Comparison of performance of two axial-flow-pump rotors for noncavitating conditions.

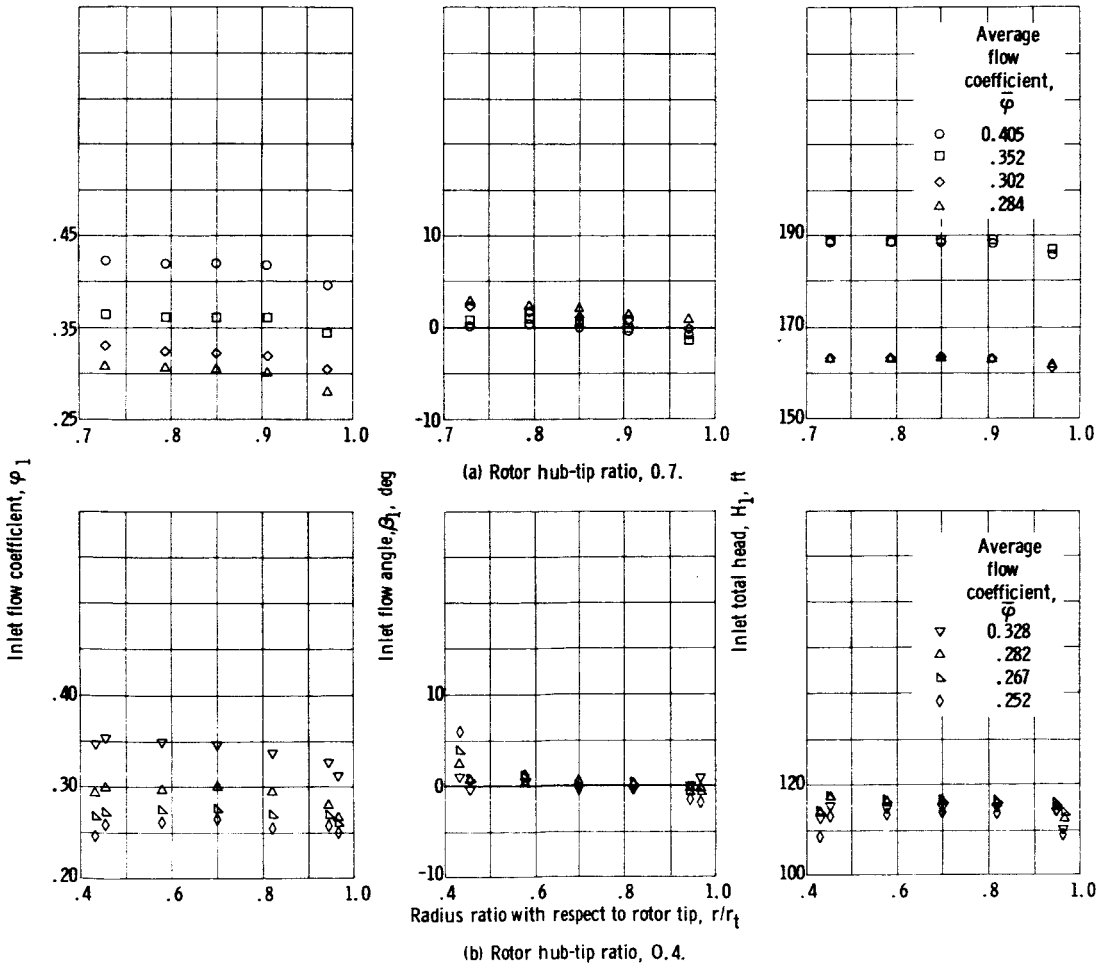


Figure 12. - Comparison of inlet radial distributions of two axial-flow-pump rotors for noncavitating conditions.

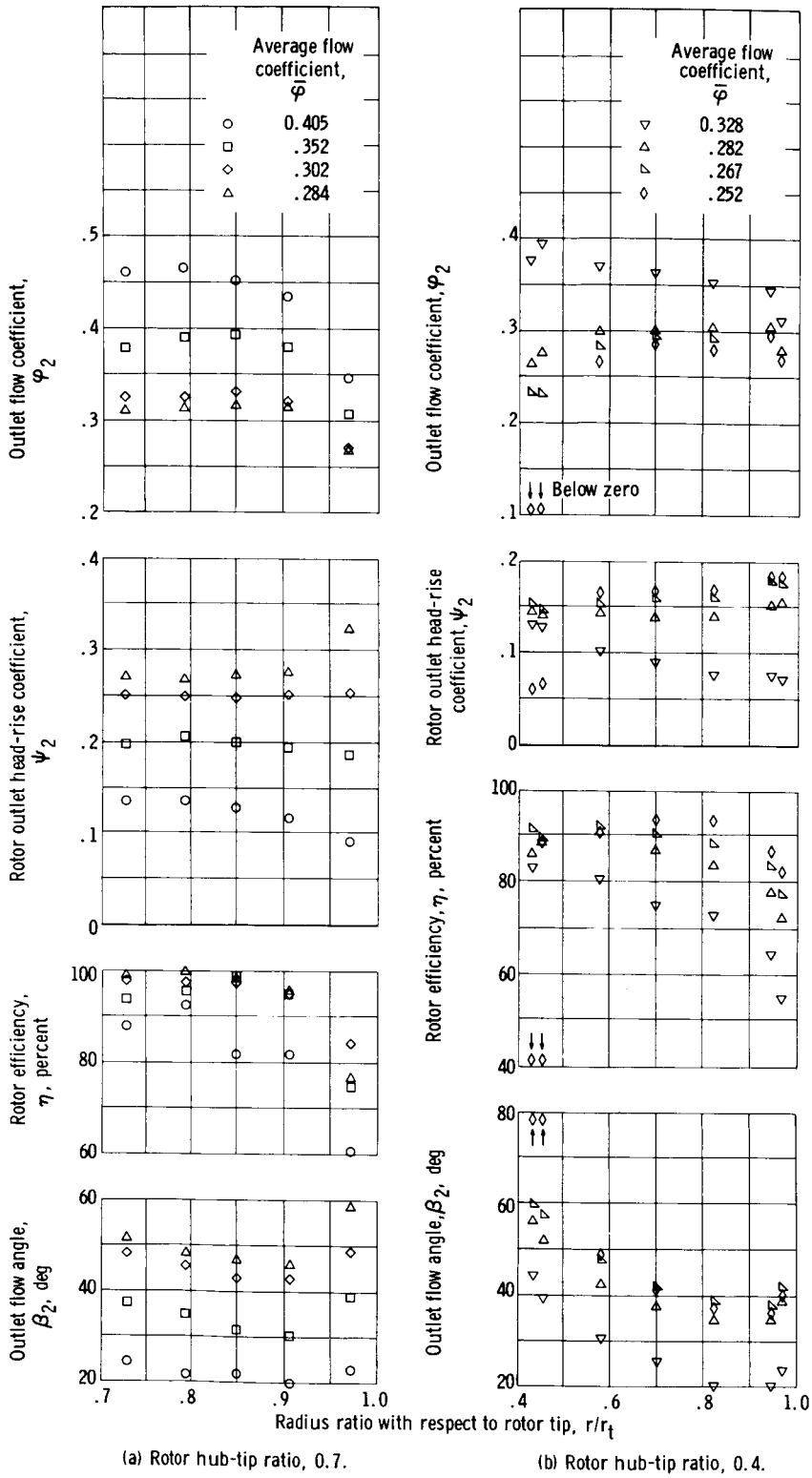


(a) Rotor hub-tip ratio, 0.7.

(b) Rotor hub-tip ratio, 0.4.

Figure 13. - Comparison of outlet radial distributions of two axial-flow-pump rotors for noncavitating conditions.

as indicated. For the more highly cambered blade (increased blade loading) used for the 0.7-hub-tip-ratio rotor, it would be anticipated that the minimum-loss incidence angles would decrease from the 3° to 4° range measured for the 0.4-hub-tip-ratio rotor, which is lightly loaded (see ref. 1). Thus, it seems likely that the 0.7-hub-tip-ratio rotor was operating close to its minimum-loss incidence angle at the design flow. This would account, in part, for the high level of efficiency at the design operating point. Furthermore, it is shown in reference 7 that the flow incidence angle margin between a reference or design point and blade stall condition decreases as the design blade loading increases. Considerations of all these factors appear to give a reasonable explanation of the relative location of the design and stall points for the two rotors. The previous comments are somewhat simplified because they do not consider what effect the performance of the individual blade elements may have on the overall results.

A comparison of the inlet radial distributions of total head, flow angle, and flow coefficient (fig. 12) indicates that similar inlet flow geometries are obtained

for the two rotors. The small inlet flow angles observed appear to justify the design assumption of no inlet whirl used in the design procedure of both rotors.

The variations in outlet radial distributions of flow angle, head-rise coefficient, and flow coefficient over a range of operating conditions are presented in figure 13.

The designs of both rotors are characterized by high inlet flow angles and radially constant energy addition (a free vortex distribution of angular momentum at rotor outlet), which, depending on radial loss distributions, results in nearly constant values of both head-rise coefficient and axial velocity. At design flow (average flow coefficient of 0.284), both rotors came reasonably close to achieving the design variation of outlet flow coefficient and head-rise coefficient. With design flow as a base point, the following discussion covers the radial distributions occurring at off-design flow conditions.

For this type of pump design, the outlet relative flow angles are highest in the tip region and decrease as radius ratio decreases. This decrease occurs because, as blade speed decreases with radius ratio, (1) the inlet relative flow angle decreases and (2) increased turning is required to maintain energy addition. Thus, a design of this type results in a radially increasing outlet relative flow angle with increasing differences between hub and tip values as radius ratio is decreased. Using the approximation that the relative outlet flow angle remains constant as flow is varied (deviation angle maintained) shows, from the analysis of typical velocity diagrams, that, for a given change in flow coefficient, greater changes in tangential velocity component $V_\theta$ (and thus in energy addition) occur at the higher outlet relative flow angles. This means that, as flow is varied from the design value, the largest change in energy addition occurs in the blade tip region and relatively smaller variations (decreasing with radius ratio) at other stations along the blade height. For example, with a relative outlet flow angle of $0^\circ$ (turning to the axial direction), any change in outlet axial velocity will not affect the energy level (outlet angular momentum) at this station.

It should be noted that, at any given flow, the combination of energy distribution and flow distribution obtained is the result of mutual interaction among the energy distribution, the equilibrium requirement, and the continuity requirement. When flow is varied from the design point at a radial station where a high energy level is produced, (compared with the radial average level) the high energy level requires an increase in the local axial velocity to fulfill equilibrium and continuity requirements. This, in turn, reduces the tendency for the local energy to increase. At a low energy station (compared with the radial average level), the converse occurs. The net result is that, as flow coefficient is varied from the design value, local values of energy level and axial velocity vary in the same direction; however, the radial gradients are somewhat less severe than they would be if these parameters acted independently.

This discussion is simplified because the effects of loss coefficient have been omitted. While the trends noted previously generally apply, they will be

tempered somewhat by effect of head loss, particularly in areas where sharp gradients of loss occur or where loss increases sharply with a change in operating mode.

The trends concerning energy addition are generally reflected by the radial variations of head-rise coefficient shown in figure 13. As flow is varied from the design value, the greatest changes in rotor head-rise coefficient occur in the tip regions for both rotors. Lesser, but significant, changes occur at a radius ratio of 0.7 (hub of the 0.7-hub-tip-ratio rotor), and only small changes show at a radius ratio of 0.4 (hub of the 0.4-hub-tip-ratio rotor).

Similarly, the trends of axial velocity noted previously are also evident from the radial variations of flow coefficient for the 0.7- and 0.4-hub-tip-ratio rotors. For instance, as flow coefficient is increased from the design value of 0.284 to a value of 0.328, the radial distributions of flow coefficient observed for the 0.4-hub-tip-ratio rotor vary markedly, while for the 0.7-hub-tip-ratio rotor the form of the curve varies only slightly. Furthermore, it may be anticipated that, if the flow range of the 0.7-hub-tip-ratio rotor could have been extended to flows below the design value, changes in radial distributions of flow coefficient would also have been small. In contrast, as the flow coefficient of the 0.4-hub-tip-ratio rotor is lowered from the design value, radial equilibrium and continuity conditions become severe enough that the axial velocity at the hub drops to zero, and a reverse flow, or eddy, region is formed. The formation of an eddy results in severe mass flow shifts, poor matching conditions for a succeeding blade row, and a possible source of instability in the flow. It should be noted that, if the operating range of either rotor could be extended to higher flows, a similar eddy would be formed in the tip region of the outlet flow.

In summary, radial equilibrium effects on a high hub-tip-ratio rotor (as illustrated by the 0.7-hub-tip-ratio rotor), as flow was varied from the design value, are small. The stable operating range from design to a minimum flow was limited by blade stall. In contrast, radial equilibrium effects at off-design conditions are relatively severe for a low-hub-tip-ratio rotor of which the 0.4-hub-tip-ratio rotor is an example. The large changes in axial velocity in the hub region would present matching problems to a succeeding blade row, and ultimately the formation of an eddy in the blade outlet hub region would limit the stable operating range rather than a blade stall condition.

## SUMMARY OF RESULTS

An axial-flow rotor with a 0.7-hub-tip ratio and design blade diffusion factors at the tip and the hub of 0.43 and 0.69, respectively, was investigated. The design, the overall performance, and the radial distributions of selected parameters indicated the following:

1. At noncavitating conditions

(a) A maximum overall head-rise coefficient of 0.292 was attained at a flow coefficient of 0.271.

(b) At the design flow coefficient of 0.284 (with the assumption of a 3-percent blockage due to casing boundary layer) an overall head-rise coefficient of 0.282 at an overall efficiency of 0.937 was observed compared with design values of 0.269 and 0.917, respectively.

(c) A feature of the range of operation covered was the small difference between design flow and a stall limited value (evidenced by excessive rig vibrations). Radial distributions of flow and performance parameters indicate that, at design flow, the blade tip region was operating at a blade loading higher than the design value. Consequently, the blade tip region probably was the first to experience stall conditions as flow was decreased (loading increased) from the design operating point. Whether the excessive rig vibrations that limited operation in the low flow range were a result of blade stall conditions in the blade tip region alone could not be determined.

2. At cavitating conditions

(a) At an operating speed of 142 feet per second, the overall head-rise coefficient did not show any effects of cavitation at any operating condition until the net positive suction head was reduced to approximately 116 feet. At a flow coefficient of 0.284 (design flow), rotor head-rise coefficient was not affected until a net positive suction head less than 89 feet was reached.

(b) Radial distributions indicate that

(1) Effects of cavitation on head-rise coefficient occur at all radii.

(2) One of the effects of cavitation is a decrease in the energy-addition capability of the rotor.

3. Simple radial equilibrium adequately describes flow conditions at the rotor outlet under all modes of operation (cavitating and noncavitating).

Lewis Research Center
National Aeronautics and Space Administration
Cleveland, Ohio, February 10, 1964

## APPENDIX A

## SYMBOLS

| | |
|---|---|
| $c$ | blade chord, in. |
| $D$ | blade diffusion factor (eq. (B3)) |
| $g$ | acceleration due to gravity, 32.2 ft/sec$^2$ |
| $H$ | total head, ft |
| $\Delta H$ | blade-element head rise, ft |
| $H_{s,v}$ | net positive suction head, $H_1 - h_v$, ft |
| $h$ | static head, ft |
| $h_v$ | vapor pressure, ft |
| $i$ | incidence angle, angle between inlet flow direction and tangent to blade mean camber line at leading edge, deg (see fig. 1) |
| $\bar{k}$ | blade cavitation number (eq. (B10)) |
| $N$ | rotative speed, rpm |
| $Q$ | flow rate, gal/min |
| $r$ | radius, ft |
| $t$ | blade thickness, in. |
| $U$ | rotor tangential velocity, ft/sec |
| $V$ | absolute velocity, ft/sec |
| $\beta$ | flow angle with respect to axial direction, deg |
| $\gamma$ | blade setting angle, angle between blade chord and axial direction, deg |
| $\delta$ | deviation angle, angle between outlet flow direction and tangent to blade mean line at trailing edge, deg (see fig. 1) |
| $\eta$ | rotor efficiency, percent |
| $\kappa$ | blade angle, angle between tangent to blade mean camber line and axial direction, deg |
| $\sigma$ | blade solidity, ratio of blade chord to blade tangential spacing |

$\varphi$ flow coefficient, $V_z/U_t$

$\Phi$ blade camber angle, deg

$\psi$ rotor head-rise coefficient, $g\ \Delta H/U_t^2$

$\omega$ rotative speed, radians/sec

$\bar{\omega}$ loss coefficient, $\Delta H_{loss}/[(V_1')^2/2g]$

Subscripts:

h hub

i ideal

max maximum

m mean

p pressure

r radial position

s suction

t tip

v measured with venturi meter

z axial component

$\theta$ tangential component

1 rotor inlet

2 rotor outlet

Superscripts:

$-$ averaged quantity

' relative

* axial velocity calculated by simple radial equilibrium

## APPENDIX B

## EQUATIONS

### Blade Element Equations

Ideal head rise (energy input):

$$\Delta H_i = \frac{U_2 V_{\theta,2} - U_1 V_{\theta,1}}{g} = \frac{U_2 V_{z,2} \tan \beta_2 - U_1 V_{z,1} \tan \beta_1}{g} \tag{B1}$$

Efficiency:

$$\eta = \frac{\Delta H}{\Delta H_i} \tag{B2}$$

Diffusion factor (ref. 4):

$$D = 1 - \frac{V_2'}{V_1'} + \frac{\Delta V_\theta'}{2\sigma V_1'} \tag{B3}$$

In both design and analysis procedures for the test rotor, at the rotor inlet and outlet measuring and/or computational stations, radial equilibrium was assumed to be achieved when the radial pressure gradient balanced the centrifugal force of the fluid due to its whirling motion, or

$$\frac{\partial h}{\partial r} = \frac{V_\theta^2}{gr} \tag{3}$$

In terms of total head and velocities, equation (3) becomes (with the radial component of velocity neglected)

$$\frac{1}{2g} \frac{\partial V_z^2}{2r} = \frac{\partial H}{\partial r} - \frac{1}{2g} \frac{\partial V_\theta}{\partial r} - \frac{V_\theta^2}{gr} \tag{B4a}$$

At the rotor outlet (station 2), the following assumptions and substitutions are utilized:

$$H_1 = \text{constant}$$

$$V_{\theta,1} = 0$$

$$H_2 = H_1 + \Delta H$$

$$\Delta H_i = \Delta H + \bar{\omega} \frac{V_1'^2}{2g} = \frac{U_2 V_{\theta,2}}{g}$$

$$V_\theta = V_z \tan \beta$$

For design purposes, it was desirable to write the equilibrium equations in terms of energy addition and loss. Equation (B4a) was written in the following form with the substitutions just listed:

$$\partial(V_{z,2})^2 = 2g\ \partial(\Delta H_i) - 2g\ \partial\left(\overline{\omega}\ \frac{V_1'^2}{2g}\right) - \frac{2g^2}{\omega^2}\ \frac{\Delta H_i^2}{r^3}\ \partial r - \frac{g^2}{\omega^2}\ \partial\left(\frac{\Delta H_i}{r}\right)^2 \qquad \text{(B4b)}$$

Selected radial distributions of ideal blade-element head rise and loss coefficient are generally used to solve equation (B4b) numerically. For a known outlet geometry, the solution is an iterative one in which continuity conditions must be satisfied.

For purposes of analysis, equation (B4a) was written in terms of measured total head and angle in the integrated form

$$\left(V^*_{z,2}\right)^2_{r+1} = \frac{2g\left(H_{2,r} - H_{2,r+1}\right) - \left(V^*_{z,2}\right)^2_r\left[\tan^2(\beta_2)_r\left(2 - \frac{r_{r+1}}{r_r}\right) + 1\right]}{\tan^2(\beta_2)_{r+1}\left(\frac{r_r}{r_{r+1}} - 2\right) - 1} \qquad \text{(B5)}$$

This integrated form assumes a linear variation of the measured parameters between adjacent radial stations.

## Overall and Averaged Parameter Equations

Mass-averaged head rise:

$$\overline{\Delta H} = \frac{\int_{r_h}^{r_t} rV_z\ \Delta H\ dr}{\int_{r_h}^{r_t} rV_z\ dr} \qquad \text{(B6)}$$

Mass-averaged efficiency:

$$\overline{\eta} = \frac{\int_{r_h}^{r_t} rV_z \eta\ dr}{\int_{r_h}^{r_t} rV_z\ dr} \qquad \text{(B7)}$$

Mass-averaged head-rise coefficient:

$$\overline{\psi} = \frac{g\,\overline{\Delta H}}{U_t^2} \tag{B8}$$

Average flow coefficient:

$$\overline{\varphi} = \frac{Q_v}{448.8\pi(r_h^2 - r_t^2)U_t} \tag{B9}$$

Blade cavitation number:

$$\overline{k} = \frac{2gH_{s,v}}{U_t^2(1 + \overline{\varphi}^2)} - \frac{\overline{\varphi}^2}{(1 + \overline{\varphi}^2)} \tag{B10}$$

## REFERENCES


1. Johnsen, Irving A., and Bullock, Robert O., eds.: Aerodynamic Design of Axial-Flow Compressors. Vol. II, NACA RM E56B03a, 1956.

2. Crouse, James E., Montgomery, John C., and Soltis, Richard F.: Investigation of the Performance of an Axial-Flow-Pump Stage Designed by the Blade-Element-Theory - Design and Overall Performance. NASA TN D-591, 1961.

3. Crouse, James E., Soltis, Richard F., and Montgomery, John C.: Investigation of the Performance of an Axial-Flow-Pump Stage Designed by the Blade-Element-Theory - Blade-Element Data. NASA TN D-1109, 1961.

4. Lieblein, Seymour, Schwenk, Francis C., and Broderick, Robert L.: Diffusion Factor for Estimating Losses and Limiting Blade Loadings in Axial-Flow-Compressor Blade Elements. NACA RM E53D01, 1953.

5. Rains, Dean A.: Tip Clearance Flows in Axial-Flow Compressors and Pumps. C.I.T., Rep. 5, 1954.

6. Sandercock, Donald M., Soltis, Richard F., and Anderson, Douglas A.: Cavitation and Noncavitation Performance of an 80.6° Flat-Plate Helical Inducer at Three Rotational Speeds. NASA TN D-1439, 1962.

7. Emery, James C., Herrig, L. Joseph, Erwin, John R., and Felix, A. Richard: Systematic Two-Dimensional Cascade Tests of NACA 65-Series Compressor Blades at Low Speeds. NACA Rep. 1368, 1958.

ERRATA

NASA TECHNICAL NOTE D-2295

DESIGN AND OVERALL PERFORMANCE OF AN AXIAL-FLOW-PUMP ROTOR WITH A BLADE TIP DIFFUSION FACTOR OF 0.43

by James E. Crouse and Donald M. Sandercock

May 1964

Page 4: The values of $\bar{\omega}$ in the table should be 0.100, .030, .025, .032, .055, .090, .150.

NASA-Langley, 1966

Issued 1-28-66